EV-ecosim: A grid-aware co-simulation platform for the design and optimization of electric vehicle charging stations

Emmanuel Balogun*, Elizabeth Buechler*, Siddharth Bhela†, Simona Onori‡, and Ram Rajagopal§

***Abstract*—To enable the electrification and decarbonization of transportation systems, it is important to understand how technologies such as grid storage, solar photovoltaic systems, and control strategies can aid the deployment of electric vehicle charging at scale. In this work, we present *EV-Ecosim*, a co-simulation platform that couples electric vehicle charging, battery dynamics, solar PV systems, grid transformers, and power distribution systems, to study the design and impacts of EV fast-charging stations. This python-based platform leverages an optional Model Predictive Control scheme with multi-fidelity capabilities for various sub-components, to simulate realistic scenarios. We demonstrate the utility of *EV-Ecosim* via a case-study, focused on economic evaluation of battery size to reduce electricity costs while considering impacts of fast charging on the power distribution grid. We present qualitative and quantitative evaluations on the battery size and develop scenario-based tables. These tables delineate the trade-offs between candidate solutions, providing comprehensive insights for decision-making under uncertainty.**

***Index Terms*—battery storage, control, fast charging, modelling, optimization, simulation**

I. Introduction

THE interactions between transportation, power systems, and consumer habits is becoming more evident as the race to decarbonize the transportation sector intensifies. Rapid deployment of electric vehicles (EVs) is projected to continue within the decade, approaching 20 million by 2030 [1]. A major deterrent to EV adoption is range anxiety, which can be alleviated by fast charging. The increasing deployment of EV fast charging stations will have significant impacts on power distribution systems by increasing voltage violations and accelerating transformer aging [2]–[4]. To alleviate grid impacts, many studies suggest Battery Energy Storage Systems (BESS) as a technology to accelerate fast charging deployment. A fundamental challenge to fast charging at scale is that objectives of various stakeholders involved in the EV charging ecosystem may not always align. Thus, to accelerate the deployment of fast-charging infrastructure, the entire EV ecosystem should be considered. For example, utilities may want to minimize voltage violations and defer distribution circuit and power transformer upgrades, while EV charging companies may want to maximize their station reliability and profit. Depending on who owns grid storage, maximizing its operational value while minimizing its degradation may be important. Since these objectives may not align, it is inherently challenging to optimize for the interests of all stakeholders in a mathematical formulation without making overtly simplified approximations.

A. Co-optimization of Electric Vehicle Service Equipment and Distributed Energy Resources

BESSs can reduce overall energy and environmental costs because of their fast response to power signals, lack of running fuel, and role in enabling the integration of other carbon-free distributed energy resources (DERs) [5]. Because DERs such as solar PV and BESS require significant capital costs, it is important for an EV charging service provider (EVSP) to size their DERs to be economical. If sized properly, BESSs can be leveraged for energy arbitrage and frequency regulation, which can reduce electricity bills and make revenue in the electricity markets to pay back its cost over its lifetime [6]–[8]. So naturally, there have been multiple research studies on the optimization of DERs for planning and operations.

In many studies, authors propose formulations for optimal sizing and operation of DERs for Electric Vehicle Supply Equipment (EVSEs), which commonly include Mixed-integer Linear Programs (MILPs). Authors in [9]–[11] propose MILPs for optimally sizing storage for a fast charging station, with the objective of minimizing overall station cost. In [7], the authors investigate the optimal sizing for residential BESS by using linear approximations to model major components, specifically the BESS. A recurring theme in these works is that they do not consider local distribution network effects and they oversimplify key subsystem models. Oversimplification of systems with nonlinear dynamics (e.g., BESS) with linear approximations may yield unwanted costs and misleading results. In [12], [13], the authors showed in an electricity market study that higher fidelity models can provide greater economic value over operational lifetimes.

B. Simulation of EVSE and DERs

Many optimization problems that study EV charging involve some form of simulation, either at the component or system level. Some models use Monte-Carlo sampling methods or statistical models to capture certain components of the problem. Due to the paucity of EV charging data, studies use models to generate EV charging load curves. Many include Gaussian

*Department of Mechanical Engineering, ‡Department of Energy Science and Engineering, and §Department of Civil and Environmental Engineering, Stanford University, Stanford, USA. †Siemens, Princeton. Author was supported by the Chevron Energy Fellowship and Stanford Bitts and Watts.

Mixture Models (GMMs) [14], [15] which perform well on an aggregate. Others have shown that deep learning (DL) generative models can learn EV load profiles and generate them with a high fidelity [16].

Co-simulation platforms provide the means to tie the interactions between EV charging, DERs, and the grid, to study EV impacts. One example of such a platform is HELICS [17], a transmission-distribution market co-simulation framework. Authors in [18] use HELICS to investigate the impacts of EV charging at scale for the San Francisco (SF) Bay Area. However, because major charging bottlenecks occur at the distribution level [3], evaluating candidate EV station configurations on local networks is critical for rapid decision-making and deployment. Additionally, the heterogeneity of distribution circuits make them critical to understanding the impact of EV charging on local community grid resilience and equity [19].

C. EV-ecosim

EV charging station design optimization with DERs is non-trivial because it must consider lifetime operation. As opposed to solving a simplified joint optimization problem for operations and system component sizing, we take a scenario-based simulation approach. This can help reduce oversimplification of non-linear systems, like batteries. To do this, we build *EV-ecosim*, a python-based multi-fidelity co-simulation environment that couples EV charging, battery system identification and degradation, power systems, and customized controls, to value pathways for scaling EV fast-charging using DERs. With *EV-ecosim's* framework, an EV charging provider can set up scenarios and configurations for solar, battery, and transformer sizes under different optimization objectives and calculate the expected costs/revenue and grid impact of different objectives at varying EVSE utilization levels.

The main contributions from this paper are as follows:

1) We introduce *EV-ecosim*, a co-simulation platform that couples EV charging with the power distribution network, transformer dynamics and aging, calibrated battery storage dynamics and aging, solar PV, and post-simulation cost estimates.
2) We include a battery system identification module with open-circuit voltage correction scheme, which significantly improves the equivalent circuit battery model.
3) We demonstrate the value of *EV-ecosim* via a use case for sizing collocated battery and solar for an EV charging station, while considering effects on the local power distribution network and economic viability.

The rest of the paper is organized as follows. In Section II, we describe the simulation framework, including components that make up the system and state evolution. In Section III, we describe a case-study that leverages *EV-ecosim*. In Section IV we discuss the results and conclude in Section V.

II. Simulation framework

Fig. 1 describes the *EV-ecosim* framework. Every subsystem is built as a module. We emulate physical systems using their respective state models and their interactions are captured via data exchange at each time step. The framework includes a controller that receives feedback from simulated physical systems. The charging simulation orchestrator initializes all modules (within the dashed region) using their respective configurations and populates all charging station modules at specific nodes in the power network.

The optimization and controller modules exist separately by design but work in unison. The controller loads the optimization module, takes as input the load signal from the load generator, and sets up the problem to be solved. Afterwards, the controller takes the solutions from the optimization module and sends control signals to the Solar and Battery modules. All desired time series for the module states are saved during and after simulation. The post-simulation cost module produces estimates for system lifetime costs and grid impact. $P_{b,ev}$ and $P_{s,ev}$ are the powers from the solar and battery system to the EVSE, respectively. I_b is the current signal from the controller to the battery. $P_{s,b}$ is the power from solar to battery. $P_{grid,b}$ is the power from the grid to the battery. Q_{cap} is the battery's capacity. T_a, T_o, and T_h are the ambient, transformer top-oil, and transformer hot-spot temperatures, respectively. We now discuss individual modules for the rest of this section.

A. Battery Dynamics

Batteries constitute a significant portion of the cost in electrification projects, accounting for about 20-30% of the overall cost of a passenger EV [20]. Using accurate models is important to maximize the value of the system. Approaches today include bucket, physics-based, and equivalent circuit models.

1) *Bucket Models (BM)*: These are the simplest and most common battery models used in optimization studies storage [7], [9]–[11], [21]. They do not model any physics.
2) *Physics-based models (PBM)*: PBMs are developed from first principles. PBMs model the internal components of the battery cell and range in complexity in the details of the components they capture. Examples of physics-based models include the single particle model (SPM), pseudo-2D model (P2D).
3) *Equivalent Circuit Model (ECM)*: Due to their computational tractability, ECMs are often used in battery management systems [22]. They are data-driven semi-empirical models that use a circuit model to capture battery dynamics, rather than modeling the physics of the battery's internal components. A well-calibrated ECM with the right context may outperform PBMs.

We elect ECMs due to their modest tradeoff between computational complexity and accuracy. The ECM consists of a single resistance R_o and two resistance-capacitor (RC) pairs; see Fig. 2. A cell is modelled and scaled by combining the cells in series and parallel to form a pack. Pack configurations can be specified by the user by setting the desired voltage and energy capacity. It is assumed the cells are maintained at constant ambient conditions at $23°C$, thus, internal thermal dynamics are not explicitly modelled in this paper.

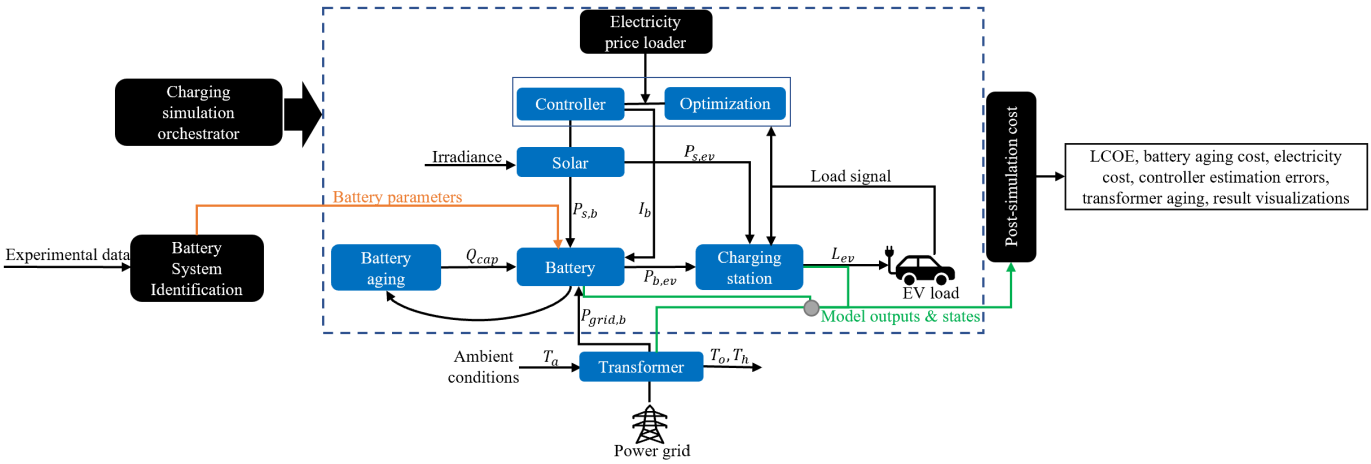

Fig. 1. System diagram for simulation framework showing the various objects and flow of inputs/outputs.

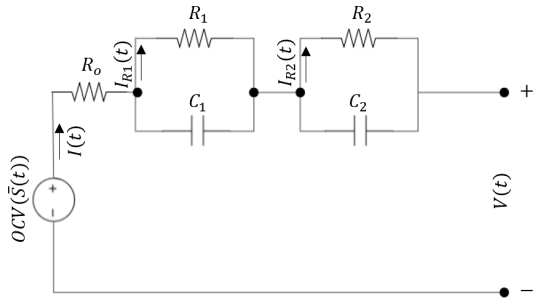

Fig. 2. ECM circuit diagram

$OCV(\bar{S}(t))$ is the open circuit voltage of the cell and a function of the battery cell's state of charge (SoC) $\bar{S}(t)$ at time t. The voltage equation for the RC-circuit in Fig. 2 is:

$$V(t) = OCV(\bar{S}(t)) - I(t)R_o - I_{R1}(t)R_1 - I_{R2}(t)R_2, \quad (1)$$

stating that the voltage across the terminals of the cell is equivalent to the open circuit voltage minus the voltage drop across the resistive components of the cell. The current flowing through R_o is the current induced by the load to which the battery is connected to, or the discharge or charge current of the battery. The power extracted from a battery at time t is:

$$P(t) = V(t)I(t). \quad (2)$$

The current flowing through R_o is $I(t)$, the load current in the cell. Each RC pair comprises a resistor and capacitor that are connected in parallel, thus the sum of the current flowing through the resistor and capacitor must be equal to the current $I(t)$ flowing into the connecting node:

$$I(t) = I_{R1}(t) + C_1 \frac{dV_{c1}}{dt} \quad (3)$$

$$I_{R1}(t) = I(t) - R_1 C_1 \frac{dI_{R1}}{dt} \quad (4)$$

dV_{c1}/dt is the rate of voltage change across capacitor C_1 and dI_{R1}/dt is the rate of current change across resistor R_1. Equations (3) and (4) hold similarly for the 2nd RC pair R2-C2, by simply replacing the indices. These relationships hold if one desires to increase the order of the ECM by including more parallel RC pairs. The battery state evolution is guided by the following equation [23]:

$$I_{R1}(t + \Delta t) = e^{-\frac{\Delta t}{R_1 C_1}} I_{R1}(t) + \left(1 - e^{-\frac{\Delta t}{R_1 C_1}}\right) I(t) \quad (5)$$

We next describe how experimental data can be used to identify realistic estimates for $R_o, ..., C_2$ which can then be used in simulation. If an *EV-ecosim* user has experimental data for the battery system they wish to simulate, this methodology can be used to produce realistic parameter estimates.

B. Battery System Identification

The battery system identification module is important for accurate representation of the battery dynamics. We demonstrate the system identification module on data from 10 identical cells, each subjected to Urban Dynamometer Driving Schedule (UDDS) cycles, Hybrid Pulse Power Characterization (HPPC), and Electrochemical Impedance Spectroscopy (EIS) diagnostic tests [24]. The cells were tested at different charging rates, ranging from C/4 to 3C, where 1C rate is equivalent to discharging the entire battery cell capacity in 1 hour.

Because of the non-linearity of ECM model equations, we use a Genetic Algorithm (GA) to learn the ECM parameters. From the experimental data, we observed that the voltage drop for a given current $I(t)$ depended on its SoC, suggesting some dependence (or correlation) of resistance with SoC. Consequently, we modelled the resistance R_o as a function of SoC with the relationship:

$$R_o(\bar{S}(t)) = B_{R_o} e^{\bar{S}(t)} + A_{R_o} e^{C_{R_o}\bar{S}(t)} \quad (6)$$

where A_{R_o}, B_{R_o}, and C_{R_o} are parameters that are learned by the GA. We feed the experimental data through our system identification module and obtain a parameter vector $\Theta = [R_1, C_1, R_2, C_2, A_{R_o}, B_{R_o}, C_{R_o}]^T$. In the GA, the objective function is called the "fitness function", which is defined as the negative RMSE of the ECM times α_{fit}:

$$J = -\alpha_{fit} \sqrt{\sum_{i=1}^{n} \frac{1}{n} \left(V_{data,i} - V(\Theta)_i\right)^2} \quad (7)$$

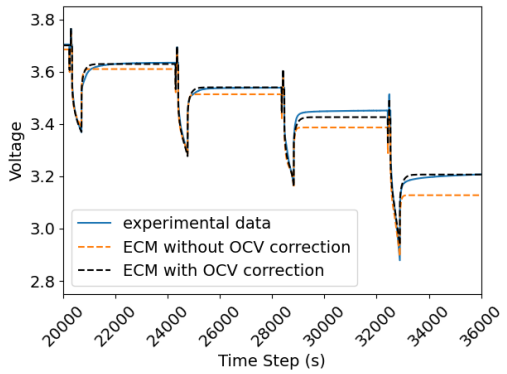

Fig. 3. Plot showing OCV correction on model accuracy

where $V_{data,i}$ is the experimental voltage and $V(\Theta)_i$ is the voltage from the ECM model. n is the number of measured data points. We introduce a hyperparameter, α_{fit}, to increase the fitness function's variance over the search space, to encourage exploration; we choose $\alpha_{fit} = 10$ and find it works well across all cells.

During fitting, there is an error on the predicted voltages across all SoC, thus we hypothesized that the constant error is induced by a bias in one of the measurements. As a result of this, we introduce a novel *open circuit voltage correction (or OCV correction)* scheme. OCV is typically measured by loading the cell with a small DC signal, usually C/20, to measure the voltage across its terminals. This is bound to underestimate the OCV because: (1) the loading device and circuit wires induce voltage drops because of their own internal resistance, and (2) it is impossible to load the cell without a voltage drop across its terminals. The steps for OCV correction are as follows:

1) Use use the initially measured OCV to fit a 2nd order ECM for the cell and save the learned parameters.
2) Using the ECM model with parameters learned from step (1), simulate the voltage response to learn the quadratic bias correction function (Equation (8)), which is a function of the original measured OCV, to produce a corrected OCV that eliminates the bias error.

$$OCV := a \cdot (OCV)^2 + b \tag{8}$$

3) Finally, run step (1) again using the learned OCV correction function to fit a new 2nd order ECM, which is the final cell model. All OCVs used in the final battery model are the corrected OCVs.

Once the learned cell parameters are passed into the battery module, the battery pack is built up into the desired series-parallel configuration. We assume all cells are identical and balanced. The battery pack is scaled up similarly as done in [25], [26]. The impedance of a parallel RC pair is $R/(1 + jRC\omega)$, which can be rewritten as $1/(1/R + jC\omega)$. For a group of n identical series impedances, the equivalent impedance for the series connected RC pairs is $1/(1/nR + jC\omega/n)$, from which we infer an equivalent resistance and capacitance, $R_{eq,s} = nR$ and $C_{eq,s} = C/n$ respectively.

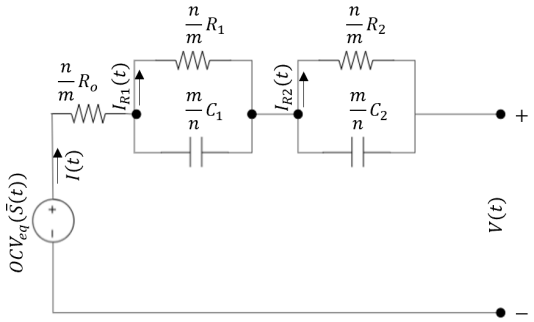

Fig. 4. Battery pack ECM diagram

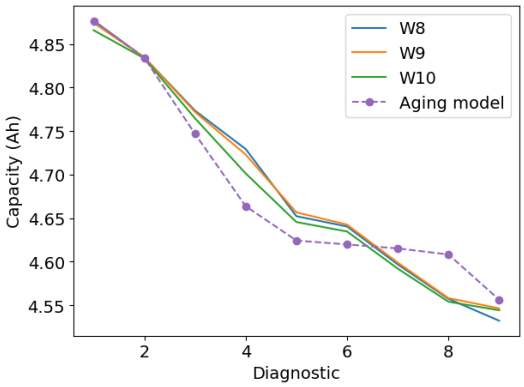

Fig. 5. Plots of experimental data of 3 NMC cells and aging model

Similarly, for a group of m identical parallel impedances, the equivalent impedance is obtained using Ohm's law as $1/(m/R + mjC\omega)$, which yields an equivalent resistance and capacitance, $R_{eq,p} = R/m$ and $C_{eq,p} = mC$.

The derived pack ECM from an initial cell model is shown in Fig. 4. n represents the number of cells in series and m is the number of modules in parallel. OCV_{eq} is the equivalent OCV ($OCV_{eq} = n \times OCV$).

C. Battery Aging

As displayed in Fig. 1, the battery aging module is distinct from the battery module. This design choice allows one to adopt and test multiple degradation models for different battery types and chemistry. It also aids easy model re-calibration and future model improvements. During each simulation time step, the aging module updates the battery module's state-of-health.

The aging model used in this paper is a semi-empirical model described in [27]. The authors showed that their model was able to extrapolate beyond the temperature conditions in the training data. In [27], aging is captured by two modes: *calendar* and *cycle* aging.

1) Calendar aging: The calendar aging of the battery occurs continuously, even when at rest. It has been shown to be temperature and voltage dependent. The temperature dependance is captured by the Arrenhius relation:

$$\alpha_T(T) = a_1 e^{\frac{-E_A}{RT}} \tag{9}$$

and the voltage dependence is represented as

$$\alpha_V(V) = a_1 V + a_2 \tag{10}$$

, where E_A is the activation energy, R is the gas constant and T is the thermodynamic temperature [27]. $\alpha_V(V)$ and $\alpha_T(T)$ are combined in [27] to obtain $\alpha_{cal}(T,V)$ and then the relation in Equation 11 is used to calculated calendar aging. Parameters a_1 and a_2 are from [27].

$$Q_{lost,cal} = \alpha_{cal}(T,V)t^{0.75} \tag{11}$$

$\alpha_{cal}(T,V)$ is a voltage and temperature dependent aging factor.

2) Cycle aging: similar to calendar aging, cycle aging factor β_{cap} is learned from experimental data and depends on the average discharge voltage and the change change in discharge depth [27]. The cycle aging function comprises the cycle aging factor β_{cap} and the total charge throughput $Q(t)$ in amp-hours (Ah) at time t.

$$Q_{lost,cyc} = \beta_{cap}\sqrt{Q} \tag{12}$$

The capacity update function obtained from equations (11) and (12) is

$$Q_{cap}(t+\Delta t) = Q_{cap}(t) - Q_{lost,cal}(t) - Q_{lost,cyc}(t) \tag{13}$$

Parameters for data-driven models are usually unique to a specific cell, so parameters must be adjusted to fit a different cell with the same chemistry. We scale the aging factors in order to achieve a comparable per-cycle loss-of-life of the cells in [24]. The aging plot is generated by using the same experimental current profile on the battery module; see Fig. 5. Each cell is subjected to a charging protocol at a specified C-rate and each diagnostic represents a capacity test after a specific number of cycles [24].

D. Transformer thermal dynamics

One of the most popular models for transformer thermal dynamics was introduced in [28], [29], and is based on a 2nd order lumped capacitance thermal model that defines the temperature changes in the oil and hotspot because of iron loss and the copper loss in the transformer. The thermal dynamics equations are given by:

$$\frac{\partial\theta_o(t)}{\partial t} = \frac{-1}{\tau_o}(\theta_o(t)-\theta_a(t))^{\frac{1}{n}} + \frac{\Delta\theta_{or}^{\frac{1}{n}}}{\tau_o}\left(\frac{K(t)^2R+1}{R+1}\right) \tag{14}$$

$$\frac{\partial\theta_h(t)}{\partial t} = \frac{-1}{\tau_h}(\theta_h(t)-\theta_a(t))^{\frac{1}{m}} + \frac{\Delta\theta_{hr}^{\frac{1}{m}}}{\tau_h}K(t)^2 \tag{15}$$

The thermal state is propagated at each time step using the Euler method. θ_h is the hot spot temperature of the transformer, θ_o is the top oil temperature, and θ_a is the ambient temperature. τ_o is the top-oil time constant and τ_h is the hotspot time constant. $K(t)$ is the ratio the of current load on the transformer at time t to the rated load of the transformer, R is the ratio of the copper loss to the iron loss at the rated load. $\Delta\theta_{or}$ is the rated change in top-oil temperature (the change in top oil temperature at the rated load) and $\Delta\theta_{hr}$ is the rated change in hot spot temperature. m and n are constants based on the expected cooling mode of the transformer. The recommended values are included in the IEEEC57-91-2011 guide for loading oil-immersed transformers [30].

E. Solar

The solar module does not explicitly model complex dynamics. It ingests configuration files that determine the system capacity and location. Solar power output is calculated using irradiance data from the NREL US solar irradiance database [31]. The output of the solar module is given by:

$$P_{solar}(t) = \min\left(P_{rated}, G_{irr}(t)A_{panel}\eta_s(t)\right) \tag{16}$$

where P_{rated} is the rated capacity of the solar PV, $G_{irr}(t)$ is the Global Horizontal Irradiance (GHI) at time t, A_{panel} is the surface area of the panel and $\eta_s(t)$ is the efficiency.

F. Charging station (EVSE)

The charging station (or EVSE) module produces a load with a power factor parameter that determines its reactive load contribution, if any. It also retains all information of all power injection at its grid node/bus. It is initialized with its location, capacity, and efficiency. The EVSE module ingests the battery, solar and controller modules to which it is assigned. The power equations for the charging station are

$$P_{grid} = P_{ev}\frac{1}{\eta_{evse}} \tag{17}$$

$$Q_{grid} = P_{ev}\tan\left(\arccos\left(pf\right)\right) \tag{18}$$

with pf as the power factor, P_{grid} and Q_{grid} are the real and reactive loads, and η_{evse} is the efficiency.

G. Power system

EV-ecosim interfaces with GridLAB-D [32], an open-source power systems modeling and simulation environment, to simulate the power distribution system. GridLAB-D is a simulator for running three-phase unbalanced quasi-static timeseries power flow calculations. The interface between *EV-ecosim* allows simulation variables to be passed between the two environments at each timestep in the simulation. At each timestep, the real and reactive power injections are calculated by *EV-ecosim* modules and sent to GridLAB-D before running the power flow calculation. GridLAB-D solves the power flow problem using a Newton-Raphson solver using the current injection method [32]. Power flow solution values can then be passed back to *EV-ecosim*, if they are used by the simulation or controller. A variety of different distribution system feeder models can be simulated in GridLAB-D, such as standard IEEE test systems [33], synthetic taxonomy feeders [34], or real-world feeder models. Such models are then populated with time-varying load profiles and DER locations. The spot loads from the original feeder models can be used to inform the placement of resources and development of time-varying load profiles.

H. Controller

The controller is a user-defined module that decides how controllable DERs are leveraged. A user can specify the controller to be of any form. It can be logic-based or optimization-based, with any objective, given it produces the relevant control variables at each time step. We allow this flexibility

TABLE I
DESCRIPTION OF CONTROLLER OPTIMIZATION VARIABLES

Variable	Description	Sign
$I_{solar}(t)$	Current from solar to battery	(+)
$I_{grid}(t)$	Current from grid to battery	(+)
I_{max}	Max allowable battery current	(+)
$I_{ev}(t)$	Current from battery for EV charging	(+)
$I(t)$	Current flow in or out of battery	(+)
$P(t)$	Power flow in or out of battery	(+, -)
$P_{ev}(t)$	Power from battery to EV	(-)
$S(t)$	Battery state of charge	(+)
$S_{ev}(t)$	Power from solar to EV	(+)
$L_{ev}(t)$	EV charging load (kW)	(+)

because it can be useful for control design. In this paper, we use an optimization based controller that solves a MILP. However, the true states of the modules are evolved using the higher fidelity models described in this paper. The unavoidable asymmetry between controllers and real systems is a desirable effect we wish to capture, as it closely mirrors reality.

The controller can work in either a Model Predictive Control (MPC) fashion or as an open-loop optimization. In the MPC mode, only the first computed action is taken before all the states are updated. Then the next optimization problem is solved at the next time step, with the current state becoming the initial state for the next problem and the horizon shifted forward one step. For the open-loop scheme, one optimization problem is solved for the entire horizon. The open-loop approach is computed offline while MPC is an online control policy that can account for model and environment uncertainty.

a) Decision variables: The main decision variables are $I(t)$, $I_{solar}(t)$, $I_{ev}(t)$, and $I_{grid}(t)$ as described in Tab. I.

b) Optimization problem: For the case study discussed Section III, the objective is to minimize the EVSE's overall electricity cost. The problem is described below as:

$$\underset{I_{solar},I_{ev},I,I_{grid}}{\text{minimize}} \quad \lambda_{elec} \tag{19}$$

$$\text{subject to} \quad \bar{S}(t=0) = \bar{S}_{initial} \tag{20}$$

$$\bar{S}(t \neq 0) = \bar{S}(t-\Delta t) + \frac{I(t)\Delta t}{Q(t)} \tag{21}$$

$$y_{solar}, y_{grid}, y_{ev} \in 0, 1 \tag{22}$$

$$I_{solar}(t) \leq I_{max} y_{solar} \tag{23}$$

$$I_{grid}(t) \leq I_{max} y_{grid} \tag{24}$$

$$I_{ev}(t) \leq I_{max} y_{ev} \tag{25}$$

$$I_{ev}, I_{solar}, I_{grid} \geq 0 \tag{26}$$

$$y_{ev} + y_{grid} \leq 1 \tag{27}$$

$$y_{ev} + y_{solar} \leq 1 \tag{28}$$

$$P_{ev}(t) = -I_{ev}(t) V(t-\Delta t) \tag{29}$$

$$P_{grid}(t) = I_{grid}(t) V(t-\Delta t) \tag{30}$$

$$P_{solar}(t) = I_{solar}(t) V(t-\Delta t) \tag{31}$$

$$P(t) = P_{ev}(t) + P_{solar}(t) + P_{grid}(t) \tag{32}$$

$$L_{ev}(t) + P_{ev}(t) - S_{ev}(t) \geq 0 \tag{33}$$

λ_{elec} will be properly defined in Section III below. The controller constraints are defined w.r.t the battery and other resources. Many of these constraints are necessary to ensure the controller is working within the space of physically realistic solutions. Equations (20)-(28) ensure the control actions respect battery physics. Equations (20)-(21) define the SoC evolution via coulomb counting. Equation (26) defines binary variables y_{solar}, y_{grid}, and y_{ev} which control whether the battery is charging from solar PV, the grid, or delivering power to the EVSE, respectively. Equations (23)-(28) define the currents flowing into and out of the battery and Equations (27)-(28) ensure that the controller does not consider solutions where the battery is discharging and charging at the same time. Equations (29)-(32) define the total power injected into or delivered by the battery and Equation (33) restricts the battery from discharging to the grid.

TABLE II
PARAMETERS FOR SOLAR LCOE ESTIMATION.

Parameter	Value
Cell Technology	Mono-Si
Package type	Glass-polymer
System type	Roof-mounted commercial scale
Location	USA (CA)
Inverter loading ratio	1.3

III. CASE STUDY

We demonstrate the utility of *EV-ecosim* via a case study. We size a battery for a site in California, USA, with a fixed 80 kW capacity solar PV installed and load profiles for the site. Solar PV is allowed to net-meter at the TOU rate given to the EVSE operator. We use the Levelized Cost of Energy (LCOE) as a metric for comparing configurations across the different scenarios. We assume a perfect forecast of the EV load and insolation as we are solving a planning problem focused on sizing a DER system for different utilization scenarios.

The levelized cost of electricity is the estimated revenue or total net expenditure required to build and operate an energy system over a specified cost recovery period [35]. In this text, we use the more general phrase "levelized cost of energy," to fit the more common "levelized cost of electricity" and "levelized cost of storage (LCOS)" under one umbrella. This is done to conveniently ascribe a combined lifetime value to the system (solar + battery) rather than each component separately. The recovery period for this study is the expected operational lifetime of the energy asset.

The levelized cost of energy or LCOE of a solar PV system is equivalent to its levelized cost of electricity. We define the LCOE for the battery system as the total lifetime net expenditure per unit energy over its operational lifetime. For the LCOE of solar calculation, we use the NREL Comparative PV LCOE Calculator [36], which takes specified values to produce LCOE estimates. Tab. II shows the set of parameters used to calculate the LCOE for the solar system in this study.

The baseline LCOE for PV is \$0.067/kWh. We used a fixed capital cost of \$345/kWh for the battery, from NREL [37]. We obtain the LCOE for the battery with the following steps:

1) Select a fixed capital cost per energy capacity.

2) Calculate the expected life of the battery post-simulation. It is calculated from the amount of degradation/aging experienced over the simulation time frame:

$$L_{exp} = \frac{0.2}{Q_{lost}} N_{sim}, \tag{34}$$

where the end of life of the battery is when the battery capacity $Q(t)$ is at 80 percent of its nameplate capacity Q_{cap}. Q_{lost} is the portion of the battery's nominal capacity that was lost during the period of simulation. N_{sim} is the number of days simulated. Therefore L_{exp} is the expected life of the battery (in days) if the aging path continues as in the simulated days.

3) Calculate the expected energy throughput of the battery over its expected lifetime. This is obtained post-simulation and described by the equation:

$$E_{exp} = E_{daily} L_{exp} \tag{35}$$

where E_{daily} is the average daily energy throughput.

4) Calculate the expected battery aging cost ($). In this work, we assume all costs due to aging incurs a cost proportional to the capital cost for capacity lost.

$$\lambda_{aging} = \lambda_{capital} \frac{Q_{lost}}{0.2} \frac{L_{exp}}{N_{sim}} \tag{36}$$

The equation above simplifies into the original capital cost of the battery, implying that the expected aging cost over its expected operational lifetime is equal to the original capital cost, which is reasonable. λ_{aging} is the aging cost and $\lambda_{capital}$ is the capital cost.

5) Calculate the total cost (normalized) over its expected life, which is the levelized cost of energy. It is cost for each unit of energy flowing through the battery during its operational life ($/kWh):

$$\lambda_{LCOE} = \frac{\lambda_{aging} + \lambda_{capital}}{E_{exp}} \tag{37}$$

A. Scenarios and configuration

We investigate the impacts and economic value of different BESS systems for a given set of scenarios. The scenario is defined by the expected utilization level and environment. The EVSE controller objective is to minimize the electricity cost.

In this case study, we consider two degrees of freedom: the maximum allowable C-rate of the battery and its energy capacity. Five C-rates ($C_{sim} = \{0.1, 0.2, 0.5, 1.0, 2.0\}$) and five capacities ($E_{sim} = \{50, 100, 200, 400, 800\}$kWh) are considered, for a total of 25 simulations per month.

The station level EV charging load profiles are generated using the SPEECh model [15] at varying levels of EV penetration (see Tab. III). The power a charging station can deliver is capped by its predetermined capacity.

For the distribution network, we use the IEEE 123 bus network [33]. Data from the Pecan Street database [38] was used to populate time-varying residential building loads within the power network. The magnitude of the residential load (e.g. number of homes) at each node was sized relative to the specified spot loads. The charging station transformers were all sized at 75 kVA, for comparing the impacts of different systems design on transformers.

TABLE III
SUMMARY LOAD CHARACTERISTICS FOR SIMULATED LOAD SCENARIO

No. EVs	Peak load (kW)	Average load (kW)
400	172	22
800	354	45
1600	424	91
3200	608	178

TABLE IV
JUNE LCOE (USD/KWH) WITH 0.1 C MAX CYCLE CONSTRAINT.

No. EVs	Base	50	100	200	400	800
400	0.2573	-0.0508	-0.0491	-0.0488	-0.0486	-0.0406
800	0.2536	0.1396	0.1399	0.1402	0.1404	0.1442
1600	0.2461	0.2271	0.2172	0.2375	0.2388	0.1657
3200	0.2432	0.2639	0.2694	0.2695	0.2694	0.2229

B. Cost function

We use the PGE BEV2-S electricity bill for business EVSE in the objective [39]. The rate structure includes a time-of-use (TOU) rate and an additional subscription charge for EVSE operators to purchase a maximum penalty-free average power that can be consumed within a 15-minute interval. The subscription charges are sold based on a block system. If a customer exceeds their allowable maximum power for any 15-minute window within a month, the customer is charged an overage fee (per kW) for each kW within the 15-minute window with the maximum power subscription exceedance. We express this electricity cost mathematically below.

$$\lambda_{sub} = \gamma_b p_b \tag{38}$$

$$\lambda_{over} = p_{over} \max_t \{P_{grid}(t) - \gamma_{block} P_{all}\}_+ \forall t \in T \tag{39}$$

$$\lambda_{tou} = \sum_{t=0}^{T} p_{tou}(t) P_{grid}(t) \tag{40}$$

$$\lambda_{elec} = \lambda_{tou} + \lambda_{over} + \lambda_{sub} \tag{41}$$

λ_{sub} is the subscription cost, γ_b is an integer decision variable, which is the number of blocks to be purchased for the month and p_b is the price per block. λ_{over} is the overage cost, p_{over} is the overage fee, P_{grid} is the net grid load from the EVSE, and P_{all} is the power allocated per block. p_{tou} is the TOU price.

IV. RESULTS AND DISCUSSION

Tab. IV contains estimates for the LCOE (electricity + battery) in dollars per kilowatt-hour ($/kWh) for June. In this case study, the solar capacity was not varied, and thus is fixed for all configurations in the cost comparison matrix. The

TABLE V
JANUARY LCOE (USD/KWH) WITH 0.1 C MAX CYCLE CONSTRAINT.

No. EVs	Base	50	100	200	400	800
400	0.2573	0.2197	0.2198	0.2202	0.2269	0.2279
800	0.2536	0.2743	0.2744	0.2745	0.2777	0.2783
1600	0.2461	0.2827	0.2723	0.2929	0.2191	0.2198
3200	0.2432	0.3031	0.3032	0.3031	0.3031	0.2565

baseline (no DER) is more expensive than the configurations with DER in most cases, except at the 3200 EV load scenario for which an 800 kWh battery capacity is needed to outperform the baseline. For the 400 EV load scenario, all BESS configurations outperform the base case. Due to low utilization in the 400 EV scenario, the system generates revenue by net metering excess solar energy, yielding net profits. With 400 and 800 EVs simulated to generate load profiles, respectively, there is no overall added benefit for the increased battery capacity, as can be observed in Fig. 6. In the 400 EV (top) scenario in Fig. 6, there is an increase in the system levelized cost (or decrease in profit)—this is because the marginal cost of the battery exceeds the marginal profit from additional capacity. However, with 1600 and 3200 EVs, respectively, the overall system cost for the simulated month reduces as the battery size is significantly increased, implying there is an added benefit of increased energy capacity—this is largely driven by the fact that higher charging loads create more opportunity for load shaping by the DER. There is a slight increase in electricity cost for the 1600 EV load scenario with 200 and 400kWh batteries in Fig. 6. This is mainly driven by sub-optimal battery control signals (incurring an intrinsic cost) due to the controller's battery model error. From Tab. IV, we report a 115.5%, 43.1%, 36.7%, 8.3%, reduction in the combined LCOE between the baseline and 800 kWh configuration, for 400, 800, 1600, and 3200 EV load scenarios, respectively. We notice a downward trend in the marginal cost savings as the scenario load increases, mainly because: (1), higher utilization levels mean there is rarely any excess solar to sell back to the grid and (2), the load peak is not coincident with peak prices, (see Fig. 8), thus inherently reducing the marginal benefit from shaping the load.

We also report the cost matrix for the month of January in Tab. V. The overall cost for operating and delivering EV charging services is in general higher for the month of January than June, mainly due to lower solar irradiance levels which limits solar PV generation. We report an 11.4%, and 10.7% decrease in system costs (compared to baseline) for 400 and 1600 EV load scenarios respectively and in general an increase in costs for the other scenarios.

These tables could inform a planner on the relative economic benefits of multiple configurations, given an EVSE's capacity and utilization levels. For example, for the 400 EV load scenario, the results suggest EV charging provider can offer low rates if the solar system is allowed to sell excess back to the grid—with the caveat that this benefit depends on distribution circuit's hosting capacity. There is a strong dependence of overall system economics on environmental conditions as well. For example, for the 400 EV scenario in June, adding a 50 kWh battery reduced the overall cost of energy (compared to the baseline) by more than 100% and yielding profits. The results for January are dramatically different, owing to the dissimilar levels of irradiation during the respective seasons. It is worth noting that the overall cost of the system is not static and the expected load profile changes over time can determine if additional DER investment will be economical for a given EV charging site.

The value of DERs to any system depends on their ability

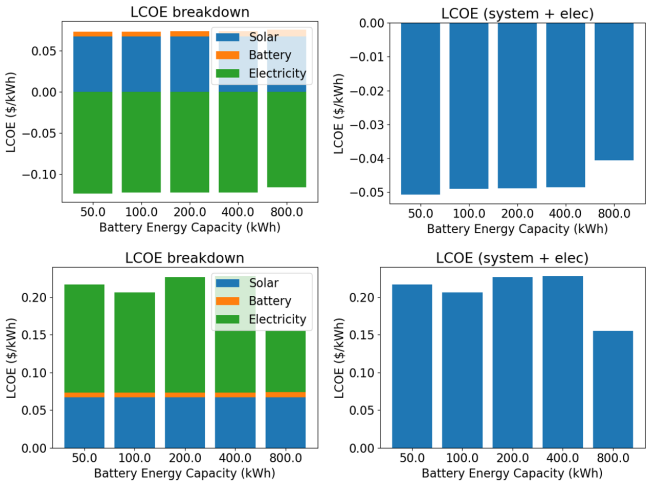

Fig. 6. Month of June top: 400EV scenario, bottom: 1600EV scenario.

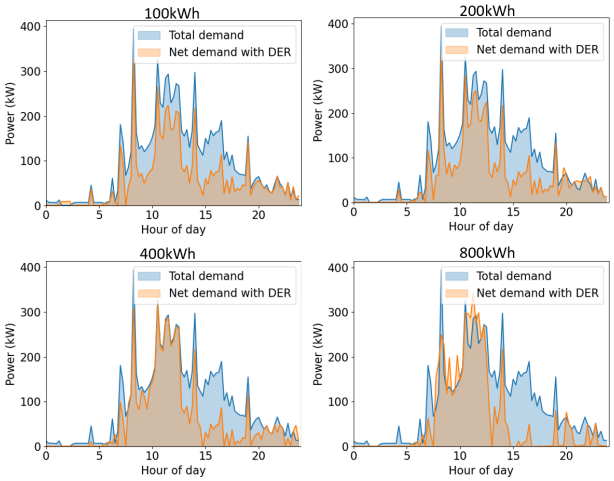

Fig. 7. Plots showing initial load and reshaped load for a day in June.

to arbitrage. As shown in Fig. 7, the load shaping ability of the system increases as the battery energy capacity increases. However, the marginal change of the load profile reduces significantly as the capacity increases, which visually explains why increasing the battery size does always not improve overall system costs in Fig 6.

A. *Transformer impacts*

We estimate the impact of EV charging from the perspective of the distribution transformers. We show the relative impacts of the different EVSE configurations on the DCFC transformer. Observe that for a fixed BESS capacity, operating the battery at a higher C-rate in general reduces transformer rating needed for that utilization level, however sometimes it can marginally depend on controller errors. Similarly for a fixed C-rate, increasing the battery size reduces transformer rating for similar utilization levels. This is because, a higher maximum discharge power allows demand spikes to be modulated. One can move along Fig. 9 to find the least cost grid feasible solution for an EVSE. For this simulation, the 800 kWh battery at a 0.5C rate has the least impact on the transformer with

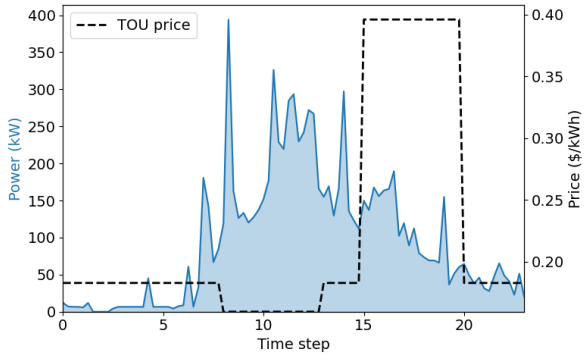

Fig. 8. Load shape for the simulated aggregate EV charging profile. The TOU rates (dotted black) show that the peak loads roughly coincide with off-peak and super-off-peak prices

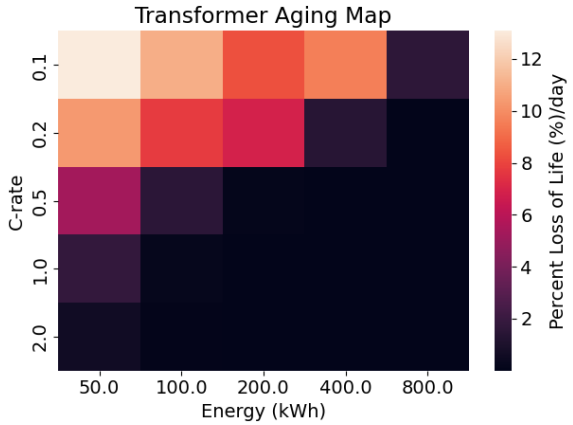

Fig. 9. Transformer aging map for 1600 EVs in June

no accelerated aging and the transformer life being preserved beyond its normal life. Meanwhile, in the worst case, it would last only a couple days. With *EV-Ecosim*, one can answer the question: *what is the least-cost system design for an EVSE with a 75kVA-rated transformer*? A user could also investigate the blended costs of the transformer, battery, solar, and grid electricity over the operational lifetime of the system.

B. Power system bus voltages

Voltage violations are defined per ANSI C84.1 standard as voltages that deviate more than 5% from the nominal. The base case with no EVSE in the network shows 0% voltage violations. The results below present the marginal effect of an EV charging system under similar grid conditions.

Tab. VI and VII show the resulting voltage violation frequency as percentages. In Tab. VI, we display the percentage voltage violations with varying maximum battery C-rates,

TABLE VI
PERCENTAGE BUS VOLTAGE VIOLATIONS IN JUNE FOR 1600EV LOAD SCENARIO WITH 50KWH BATTERY

Battery C-rate	0.1	0.2	0.5	1	2
% violations	0.0204	0.0160	0.0000	0.0000	0.0000

TABLE VII
PERCENTAGE BUS VOLTAGE VIOLATIONS FOR JUNE 1600 EV LOAD SCENARIO WITH C-RATE 0.1 C

Battery capacity (kWh)	50	100	200	400	800
% violations	0.0204	0.0160	0.0067	0.0000	0.0000

while in Tab. VII, the C-rate is fixed and the battery capacity is varied. We observe that at a fixed 0.1C rate, voltage violation frequency reduced with increased capacity, with the 400 kWh and 800 kWh batteries completely avoiding violations. The EVSE responds to prices, which are higher in the evening (see Fig. 8) and uncontrollable residential loads exist within the network, which are much higher in the evening as well. Consequently, the battery is incentivized to offset the coincident EV load and residential peak load. Notice in Fig. 7, the the larger batteries shave more of the evening load.

By investigating the combined economic ramifications for load scenarios, environmental conditions, and grid impacts, one can select the best battery size for a specific use-case. For instance, from the results displayed in this text, if the 1600 EV load scenario generated is the most likely, then the 800 kWh will be the best choice from the perspective of the combined LCOE, transformer, and grid impacts.

V. CONCLUSION

We introduced *EV-ecosim*, a Python-based co-simulation platform that couples DER subsystems with local distribution networks. It performs post-simulation economic and grid-impact analysis to aid EV operators and planners to size assets in the most grid-feasible and economic way. We demonstrated the capability of *EV-ecosim* via a case study to evaluate collocated battery storage for an EV charging station.

In real-time, model-based controllers perform calculations on lower-order (or lower fidelity) models due to computational constraints. Many existing studies do not consider the unavoidable asymmetry that can exist between the actual physical system and the models many linear controllers would adopt, leading to irreducible errors that can change the economics of the system significantly. Using *EV-Ecosim* in future work, we can demonstrate this by examining varying levels of controller model fidelity, to show that limitations in battery models can yield unintuitive results that would otherwise be lost.

The insights gleaned from co-simulation platforms are limited by the fidelity of all the underlying models, and the accuracy of the modelled interplay between critical physical systems in simulation. With *EV-ecosim*, we can conveniently improve various subcomponent models as higher quality data becomes available, underlying physics are better understood, and computational efficiency continues to improve, significantly accelerating system design and paving the pathway to deploy EV charging systems economically and equitably.

REFERENCES

[1] "Global EV outlook 2022 – analysis - IEA." [Online]. Available: https://www.iea.org/reports/global-ev-outlook-2022

[2] M. Muratori, "Impact of uncoordinated plug-in electric vehicle charging on residential power demand," *Nature Energy*, vol. 3, no. 3, pp. 193–201, mar 2018. [Online]. Available: http://www.nature.com/articles/s41560-017-0074-z

[3] B. Borlaug, M. Muratori, M. Gilleran, D. Woody, W. Muston, T. Canada, A. Ingram, H. Gresham, and C. McQueen, "Heavy-duty truck electrification and the impacts of depot charging on electricity distribution systems," *Nature Energy*, vol. 6, no. 6, pp. 673–682, jun 2021. [Online]. Available: http://www.nature.com/articles/s41560-021-00855-0

[4] S. Powell, E. C. Kara, R. Sevlian, G. V. Cezar, S. Kiliccote, and R. Rajagopal, "Controlled workplace charging of electric vehicles: The impact of rate schedules on transformer aging," *Applied Energy*, vol. 276, p. 115352, oct 2020. [Online]. Available: https://linkinghub.elsevier.com/retrieve/pii/S0306261920308643

[5] T. Terlouw, T. AlSkaif, C. Bauer, and W. van Sark, "Multi-objective optimization of energy arbitrage in community energy storage systems using different battery technologies," *Applied Energy*, vol. 239, pp. 356–372, apr 2019. [Online]. Available: https://linkinghub.elsevier.com/retrieve/pii/S0306261919302478

[6] C. Brivio, S. Mandelli, and M. Merlo, "Battery energy storage system for primary control reserve and energy arbitrage," *Sustainable Energy, Grids and Networks*, vol. 6, pp. 152–165, jun 2016. [Online]. Available: http://linkinghub.elsevier.com/retrieve/pii/S2352467716300017

[7] H. C. Hesse, M. Schimpe, D. Kucevic, and A. Jossen, "Lithium-ion battery storage for the grid—a review of stationary battery storage system design tailored for applications in modern power grids," *Energies*, vol. 10, no. 12, p. 2107, 2017.

[8] H. Hesse, V. Kumtepeli, M. Schimpe, J. Reniers, D. Howey, A. Tripathi, Y. Wang, and A. Jossen, "Ageing and efficiency aware battery dispatch for arbitrage markets using mixed integer linear programming," *Energies*, vol. 12, no. 6, p. 999, mar 2019. [Online]. Available: https://www.mdpi.com/1996-1073/12/6/999

[9] S. Negarestani, M. Fotuhi-Firuzabad, M. Rastegar, and A. Rajabi-Ghahnavieh, "Optimal sizing of storage system in a fast charging station for plug-in hybrid electric vehicles," *IEEE Transactions on Transportation Electrification*, vol. 2, no. 4, pp. 443–453, dec 2016. [Online]. Available: http://ieeexplore.ieee.org/document/7460088/

[10] G. Liu, Y. Xue, M. S. Chinthavali, and K. Tomsovic, "Optimal sizing of PV and energy storage in an electric vehicle extreme fast charging station," in *2020 IEEE Power & Energy Society Innovative Smart Grid Technologies Conference (ISGT)*. IEEE, feb 2020, pp. 1–5. [Online]. Available: https://ieeexplore.ieee.org/document/9087792/

[11] V. Salapic, M. Grzanic, and T. Capuder, "Optimal sizing of battery storage units integrated into fast charging EV stations," in *2018 IEEE International Energy Conference (ENERGYCON)*. IEEE, jun 2018, pp. 1–6. [Online]. Available: https://ieeexplore.ieee.org/document/8398789/

[12] J. M. Reniers, G. Mulder, S. Ober-Blöbaum, and D. A. Howey, "Improving optimal control of grid-connected lithium-ion batteries through more accurate battery and degradation modelling," *Journal of power sources*, vol. 379, pp. 91–102, mar 2018. [Online]. Available: http://linkinghub.elsevier.com/retrieve/pii/S0378775318300041

[13] J. M. Reniers, G. Mulder, and D. A. Howey, "Unlocking extra value from grid batteries using advanced models," *Journal of power sources*, vol. 487, p. 229355, mar 2021. [Online]. Available: https://linkinghub.elsevier.com/retrieve/pii/S0378775320316438

[14] J. Quiros-Tortos, A. N. Espinosa, L. F. Ochoa, and T. Butler, "Statistical representation of EV charging: real data analysis and applications," in *2018 Power Systems Computation Conference (PSCC)*. IEEE, jun 2018, pp. 1–7. [Online]. Available: https://ieeexplore.ieee.org/document/8442988/

[15] S. Powell, G. V. Cezar, and R. Rajagopal, "Scalable probabilistic estimates of electric vehicle charging given observed driver behavior," *Applied Energy*, vol. 309, p. 118382, mar 2022. [Online]. Available: https://linkinghub.elsevier.com/retrieve/pii/S0306261921016214

[16] R. Buechler, E. Balogun, A. Majumdar, and R. Rajagopal, "EVGen: Adversarial networks for learning electric vehicle charging loads and hidden representations," *arXiv*, 2021. [Online]. Available: https://arxiv.org/abs/2108.03762

[17] B. Palmintier, D. Krishnamurthy, P. Top, S. Smith, J. Daily, and J. Fuller, "Design of the HELICS high-performance transmission-distribution-communication-market co-simulation framework," in *2017 Workshop on Modeling and Simulation of Cyber-Physical Energy Systems (MSCPES)*. IEEE, apr 2017, pp. 1–6. [Online]. Available: https://ieeexplore.ieee.org/document/8064542/

[18] N. V. Panossian, H. Laarabi, K. Moffat, H. Chang, B. Palmintier, A. Meintz, T. E. Lipman, and R. A. Waraich, "Architecture for co-simulation of transportation and distribution systems with electric vehicle charging at scale in the san francisco bay area," *Energies*, vol. 16, no. 5, p. 2189, feb 2023. [Online]. Available: https://www.mdpi.com/1996-1073/16/5/2189

[19] A. M. Brockway, J. Conde, and D. Callaway, "Inequitable access to distributed energy resources due to grid infrastructure limits in california," *Nature Energy*, vol. 6, no. 9, pp. 892–903, 2021.

[20] "Electric vehicle battery costs soar - IER." [Online]. Available: https://www.instituteforenergyresearch.org/renewable/electric-vehicle-battery-costs-soar/

[21] Q. Yan, B. Zhang, and M. Kezunovic, "Optimized operational cost reduction for an EV charging station integrated with battery energy storage and PV generation," *IEEE transactions on smart grid*, vol. 10, no. 2, pp. 2096–2106, mar 2019. [Online]. Available: https://ieeexplore.ieee.org/document/8242670/

[22] R. Ahmed, J. Gazzarri, S. Onori, S. Habibi, R. Jackey, K. Rzemien, J. Tjong, and J. LeSage, "Model-based parameter identification of healthy and aged li-ion batteries for electric vehicle applications," *SAE International Journal of Alternative Powertrains*, vol. 4, no. 2, pp. 233–247, 2015.

[23] G. L. Plett, *Battery management systems, Volume I: Battery modeling*. Artech House, 2015, vol. 1.

[24] G. Pozzato, A. Allam, and S. Onori, "Lithium-ion battery aging dataset based on electric vehicle real-driving profiles." *Data in brief*, vol. 41, p. 107995, apr 2022. [Online]. Available: http://dx.doi.org/10.1016/j.dib.2022.107995

[25] S.-T. Ko, J. Lee, J.-H. Ahn, and B. K. Lee, "Innovative modeling approach for li-ion battery packs considering intrinsic cell unbalances and packaging elements," *Energies*, vol. 12, no. 3, p. 356, jan 2019. [Online]. Available: http://www.mdpi.com/1996-1073/12/3/356

[26] M. H. Abbasi and J. Zhang, "Joint optimization of electric vehicle fast charging and DC fast charging station," in *2021 International Conference on Electrical, Computer and Energy Technologies (ICECET)*. IEEE, dec 2021, pp. 1–6. [Online]. Available: https://ieeexplore.ieee.org/document/9698541/

[27] J. Schmalstieg, S. Käbitz, M. Ecker, and D. U. Sauer, "A holistic aging model for li(NiMnCo)o2 based 18650 lithium-ion batteries," *Journal of power sources*, vol. 257, pp. 325–334, jul 2014. [Online]. Available: http://linkinghub.elsevier.com/retrieve/pii/S0378775314001876

[28] G. Swift, T. Molinski, R. Bray, and R. Menzies, "A fundamental approach to transformer thermal modeling. II. field verification," *IEEE Transactions on Power Delivery*, vol. 16, no. 2, pp. 176–180, apr 2001. [Online]. Available: http://ieeexplore.ieee.org/document/915479/

[29] G. Swift, T. Molinski, and W. Lehn, "A fundamental approach to transformer thermal modeling. i. theory and equivalent circuit," *IEEE Transactions on Power Delivery*, vol. 16, no. 2, pp. 171–175, apr 2001. [Online]. Available: http://ieeexplore.ieee.org/document/915478/

[30] "C57.91-2011 - IEEE guide for loading mineral-oil-immersed transformers and step-voltage regulators |IEEE standard |IEEE xplore." [Online]. Available: https://ieeexplore.ieee.org/document/6166928

[31] "Nsrdb." [Online]. Available: https://nsrdb.nrel.gov/

[32] D. P. Chassin, K. Schneider, and C. Gerkensmeyer, "GridLAB-d: An open-source power systems modeling and simulation environment," in *2008 IEEE/PES Transmission and Distribution Conference and Exposition*. IEEE, apr 2008, pp. 1–5. [Online]. Available: http://ieeexplore.ieee.org/document/4517260/

[33] W. H. Kersting, "Radial distribution test feeders," *IEEE Transactions on Power Systems*, vol. 6, no. 3, pp. 975–985, 1991.

[34] K. P. Schneider, Y. Chen, D. Engle, and D. Chassin, "A taxonomy of north american radial distribution feeders," in *2009 IEEE Power & Energy Society General Meeting*. IEEE, 2009, pp. 1–6.

[35] . US EIA, "Levelized costs of new generation resources in the annual energy outlook 2022," Tech. Rep., mar 2022.

[36] "Comparative PV LCOE calculator |photovoltaic research |NREL." [Online]. Available: https://www.nrel.gov/pv/lcoe-calculator/

[37] W. Cole, A. Frazier, and C. Augustine, "Cost projections for utility-scale battery storage: 2021 update," Golden, CO (United States), Tech. Rep., jun 2021. [Online]. Available: https://www.osti.gov/servlets/purl/1786976/

[38] O. Parson, G. Fisher, A. Hersey, N. Batra, J. Kelly, A. Singh, W. Knottenbelt, and A. Rogers, "Dataport and nilmtk: A building data set designed for non-intrusive load monitoring," in *2015 ieee global conference on signal and information processing (globalsip)*. IEEE, 2015, pp. 210–214.

[39] "ELECTRIC SCHEDULE EV sheet 1." [Online]. Available: https://www.pge.com/{en_US}/residential/rate-plans/rate-plan-options/electric-vehicle-base-plan/electric-vehicle-base-plan.page